Materials Advances

ROYAL SOCIETY OF CHEMISTRY

PAPER

View Article Online
View Journal | View Issue

Cite this: *Mater. Adv.*, 2024, 5, 6114

Thin multifunctional coatings for textiles based on the layer-by-layer application of polyaromatic hybrid nanoparticles†

Sahar Babaeipour, [a] Paula Nousiainen, [a] Erfan Kimiaei, [a] Jenni Tienaho, [b] Nadine Kohlhuber, [c] Risto Korpinen, [d] Kalle Kaipanen[d] and Monika Österberg *[a]

The textile industry is striving to develop versatile coatings, combining antibacterial, water-repellent, and breathable properties, all while avoiding toxic components. However, the current solutions have unfavorable ecological impacts. Although the use of waxes has offered promise and is an eco-friendly option, there remains a challenge in achieving all the desired properties in a single solution. Here, we employed biobased nanoparticles, produced from natural fatty acid, tall oil fatty acid (TOFA) and lauric acid (La) esterified lignins and waxes, to create multifaceted textile coatings using a layer-by-layer deposition method. Our results reveal that even at nanoscale thickness, the developed coatings enhanced the water contact angle (WCA) of fabrics from 43° to ~150° while maintaining good breathability (air permeability ranging between 23 and 31 mm/s. Moreover, the coated fabrics maintained excellent hydrophobicity even after two washing cycles. The surface morphology and roughness of the coatings characterized by scanning electron microscopy (SEM) and atomic force microscopy (AFM) showed a defect-free and integrated coating layer. Additionally, the polyaromatic molecules integrated into the coatings contributed to the textiles' antibacterial properties against *S. aureus* (~50% inhibition rate) and improved UV-shielding properties, demonstrating the potential for tailored functionality based on specific application requirements. Our systematic correlation of chemical structure and particle properties enabled a comprehensive understanding of their influence on the functionality and performance of coated fabrics. Furthermore, the layer-by-layer method utilizing biobased particles is a simple and efficient method to enhance the performance of cellulose-based materials. This positions the approach as a promising solution for widespread multifunctional textile applications, such as outdoor clothing.

Received 30th January 2024,
Accepted 11th June 2024

DOI: 10.1039/d4ma00085d

rsc.li/materials-advances

1. Introduction

The textile industry is actively pursuing the development of simple multifunctional coatings that are non-toxic antibacterial, stain-resistant, water-repellent, and UV-protective.[1,2] These functional textiles can be used in various applications, such as military textiles,[3] smart electronic textiles,[4] healthcare textiles,[5] and outdoor protective wear.[6]

In recent studies, inorganic metals like palladium,[7] silver nanoparticles[8] and synthetic organic compounds such as fluorocarbon chemicals have demonstrated efficiency in enhancing antibacterial properties, UV shielding, and water repellency. However, these materials raise substantial environmental concerns.[9,10] These concerns have led researchers to explore alternative approaches that prioritize sustainability and minimize adverse environmental impacts.[11]

Biobased materials have been investigated as more sustainable solutions for post-treatment in textile finishing. Recently, biobased polyphenolic materials have gained significant attention in the textile industry. This increased interest is primarily due to their excellent biocompatibility and diverse functionalities, such as UV protection, antioxidant properties, flame retardancy, and antibacterial effects.[12] Notably, lignin and its

[a] *Department of Bioproducts and Biosystems, Aalto University, Vuorimiehentie 1, FI-02150 Espoo, Finland. E-mail: monika.osterberg@aalto.fi*
[b] *Natural Resources Institute Finland, Production Systems, Food and Bioproducts, Latokartanonkaari 9, FI-00790 Helsinki, Finland*
[c] *Institute of Chemistry of Renewable Resources, Department of Chemistry, University of Natural Resources and Life Sciences, (BOKU), Vienna, Konrad-Lorenz-Strasse 24, 3430 Tulln an der Donau, Austria*
[d] *Natural Resources Institute Finland, Production Systems, Biomass Fractionation Technologies, Viikinkaari 9, FI-00790 Helsinki, Finland*

† Electronic supplementary information (ESI) available. See DOI: https://doi.org/10.1039/d4ma00085d

derivatives, one of the most abundant polyphenolic compounds and byproducts of the pulp and paper industry, have gained interest as potential biobased solutions to impart textiles with UV-blocking and antibacterial properties.[13] The advantages of lignin are its high availability and affordability. Sunthornvarabhas *et al.* (2019) highlighted the antibacterial activity of a lignin-coated cloth against *Staphylococcus epidermidis*, which underlines the feasibility of replacing silver nanoparticles with lignin in antimicrobial textiles.[14] In Petkovska *et al.*'s (2022) work, cotton was functionalized with a lignin-containing coating, which acted as an efficient UV-blocker, attributed to the abundance of UV-absorbing chromophore groups.[15] However, lignin derived from the pulping process is too hydrophilic to work as such for improving the water repellency of textiles. Consequently, lignin is often chemically modified to improve properties like hydrophobicity, solubility, oxidative and photothermal stability, molecular mobility, and compatibility with other polymers.[16,17] For example, the hydroxyl groups of lignin can be esterified to improve its hydrophobicity.[18,19] Hult *et al.* (2013) coated paperboard with tall oil fatty acid (TOFA) esterified lignin, which resulted in significant improvement of packaging material hydrophobicity and barrier properties.[18]

Natural waxes such as beeswax and carnauba have been used for coating applications.[20,21] For instance, Janesch *et al.* (2020) successfully developed a superhydrophobic coating on wood combining beeswax and tung oil solution.[22] However, waxes derived from pine and spruce trees have been overlooked despite their versatile potential for use as building blocks, except for a few studies. Beluns *et al.* (2022) coated nano paper using pine needle wax dissolved in organic solvents by spray-coating and dip-coating methods.[23]

A predominant focus in existing research involves the utilization of wax solutions.[22] Recognizing the inherent challenge associated with the water insolubility of lignin and waxes in the context of solution coating,[24,25] we note that the application of particle coating can effectively address this issue. This alternative approach provides key benefits such as higher water repellency, breathability, and lower emission of volatile organic compounds.[26,27] There are a few examples where this approach has been successfully employed. Henn *et al.* (2021) crosslinked lignin nanoparticles with an epoxy to create a multiprotective particulate coating for wood. The particle morphology provided efficient water repellency and breathability for the wooden substrate.[24] Similarly, Moreno *et al.* (2023) developed hybrid particles using Urushi and lignin to produce multifunctional hydrophobic protective coatings.[27] However, the chemical crosslinking used in these studies is not applicable to textiles and wearables. In contrast, Forsman *et al.* (2017) achieved a combination of high hydrophobicity and breathability in textile coatings by utilizing carnauba wax particles, but the washing fastness of the coating was poor.[25]

Despite the significant contributions of synthetic chemicals to various research advancements, there remains a noticeable gap in the systematic investigation of polyaromatic particles and the relationship between the structure, properties, and applications of biobased materials in sustainable textile coatings. The novelty of this work lies in incorporating natural fatty acids into the lignin and then forming hybrid lignin particles, enhancing their hydrophobicity compared to unmodified LNPs, while also providing antibacterial, self-cleaning, and UV-blocking properties.

In this study, we created multifunctional coatings using polyaromatic particles comprised of modified hybrid lignin nanoparticles. These particles were used to produce 100% biobased coatings on cellulose nanofiber films (CNF) and on cotton fabric. The obtained coatings and their properties were further compared to coatings consisting of wax particles from commercial carnauba wax and domestic spruce needle wax. The layer-by-layer method was used to create self-assembled multilayers on cotton textiles by dip-coating. The particle-based coatings provided dual functions, modifying both the textile surface morphology and chemistry. The incorporation of natural fatty acids in the hybrid lignin particles improved the cotton fabric's hydrophobicity and provided it with antibacterial, self-cleaning, and UV-blocking properties. Additionally, the application of particulate coating dispersion to the fabric enhances the coating spreadability and provides excellent surface coverage, while maintaining its breathability.

2. Experimental

2.1 Materials

The solvents used in this study included tetrahydrofuran (THF, VWR, stabilized, 99.8%), pyridine (Sigma-Aldrich, 99.8%), chloroform (Sigma-Aldrich, 99.8%), and ethanol (Altia, 99.9%). Other chemicals used were poly-L-lysine (Sigma-Aldrich, 0.1%), kraft lignin BioPiva 395, 95% dry matter, obtained from UPM, (Lappeenranta, Finland), TOFA (a distilled fraction with 98% C18 fatty acid purity) obtained from Forchem (Rauma, Finland), dodecanoyl chloride (Sigma-Aldrich, 97.5%), thionyl chloride (Sigma-Aldrich, 97%), and Celite® 545 (Supelco, filter aid, particle size 0.02–0.1 mm).

Spruce needle wax was obtained from the Natural Resources Institute Finland (Luke). Norway spruce needle fraction was oven-dried at 60 °C overnight and extracted using a supercritical fluid pilot plant (Chematur Ecoplanning, Pori, Finland). Approximately 1 kg of plant material was charged into a vessel and placed into a closed reactor. The pressure in the reactor was gradually increased to 350 bar, the temperature was adjusted to 60 °C, and the flow rate of the supercritical carbon dioxide was 0.45 l min^{-1}. Two identical extractions were carried out, and the resulting extracts were collected and weighed at 15 min intervals to determine the endpoint of the extraction, which was reached at 105 min. The average yield of wax in the two extractions was 1.7%. The obtained extract was further purified by repeated dissolution in a small amount of hot 99.5% ethanol (ETAX Aa, Anora Group, Finland) and freezing at −20 °C overnight. The solidified wax fraction was separated by centrifugation (10 min at 2000 rpm) and siphoning, followed by washing with cold 99.5% w/w ethanol and centrifugation.

This procedure was repeated several times to remove the green color from the fraction.

The refined carnauba wax (No1, yellow, m.p. 82–84 °C) was purchased from Sigma-Aldrich (Steinheim, Germany). Carnauba wax consists of C26–C30 fatty acid aliphatic esters, diesters, alcohols, and aromatic acids.[25]

2.2 Preparation of derivatized lignin

2.2.1 Esterification with octanoic acid. Esterification of lignin was performed according to Koivu *et al.* (2016)[23] by dissolving 1.0 g of lignin in 10 ml of THF, 0.7 ml of dimethylformamide (DMF) and 0.78 ml of pyridine (all the solvents used were anhydrous). The lignin was allowed to dissolve completely in an N_2 atmosphere for 1 hour. Three different mol equivalents (eq.) of dodecanoyl chloride – 1.3, 0.7, and 0.3 eq., with respect to the amount of hydroxyl groups (mmol g^{-1}) in the lignin sample (5.4 mmol g^{-1} of phenolic and aliphatic OHs as determined by quantitative ^{31}P NMR analysis) were used for esterification to obtain samples with varying degrees of substitution. The products were named accordingly as La-L_{30}, La-L_{70} and La-L_{100}. The dodecyl chloride was slowly added to the dissolved lignin. The esterification was carried out at 60 °C, under stirring with reaction times varying from 48 to 72 hours. The purification of the esterified lignin started with adding Celite 535 to the reaction until the mixture became powdery. The product was then washed, under filtration, with cold water and ethanol. The washed powder was left to dry overnight. The product was extracted from Celite *via* Soxhlet extraction using 250 ml of THF as a solvent.[28] The esterified lignins were analyzed by ^{1}H NMR, HSQC for structural analysis, and ^{31}P NMR for analysis of remaining hydroxyl groups in the samples and determination of their degree of substitution.

2.2.2 Esterification with tall oil fatty acids (TOFA). The TOFA chlorides (TOFA-Cl) were synthesized by reacting 10 g TOFA (30 mmol, estimated by the fatty acid mixture as an average of C18 fatty acids) with an excess (8 g, 40 mmol) of thionyl chloride under reflux for 1 hour. The product was purified by distilling the excess thionyl chloride using a microdistillation system. The obtained TOFA-Cl was analyzed by NMR. The TOFA esterification of lignin was performed by adding 5 g of lignin (5.4 mmol g^{-1} of OH groups) in 30 ml dry THF, 7.5 ml DMF, and 3.9 ml pyridine and stirred for 30 min at 60 °C in a N_2 atmosphere. TOFA-Cl was added (1.3 eq. based on the phenolic and aliphatic OH groups) to the lignin solution for esterification. The reaction was kept at 60 °C in a nitrogen atmosphere for 48 hours with efficient stirring. Isolation of the esterified lignin was done as previously described.[28] The isolated TOFA-lignin was further analyzed using ^{1}H NMR, HSQC, and ^{31}P NMR.

2.3 Structural characterization of the starting materials and derivatized lignins

2.3.1 Fourier transform infrared spectroscopy (FTIR). FTIR-ATR spectroscopy was used to determine the chemical composition of the starting materials and the derivatized lignins. The spectra were acquired using a PerkinElmer Spectrum Two spectrometer (Waltham, MA, USA). The data were recorded over a wave number range from 500 cm^{-1} to 4000 cm^{-1} with 10 accumulation scans and 4 cm^{-1} resolution.

2.3.2 Gas chromatography combined with flame ionization detector (GC-FID) or mass spectrometry (GC–MS). The spruce wax and TOFA were analyzed using capillary chromatography, GC-FID for quantitative component analysis, and GC–MS for identification of the compounds. The MS spectra were referenced to the NIST (NIST17-1) spectral library. The samples (1 mg) were dissolved in 1,4-dioxane (100 μl), whereupon pyridine (10 μl), and finally, *N*,*O*-bis(trimethylsilyl)trifluoroacetamide (BSTFA) with 10% trimethylchlorosilane (50 μl) was added. The mixture was heated at 60 °C for 15 minutes while shaken occasionally. The samples were filtered using 0.45 μm syringe filters and analyzed immediately using Shimadzu GC-FID 6890 equipped with an autosampler and FID detector. The samples were injected into a capillary column (Agilent HP-5MS (5%-phenyl)-methylpolysiloxane, 30 m × 0.250 mm × 0.25 μm film) with injector temperature of 280 °C, and the compounds were separated using carrier gas at 1.0 ml min^{-1}, 80 °C initial temperature isocratic for 5 min, followed by gradient with 4 °C min^{-1} until reaching 300 °C, and finally keeping run isocratic at that temperature for 20 minutes. The GC–MS analysis was done using Shimadzu GCMS-QP2010 SE equipment with Agilent HP-5MS (5%-phenyl)-methylpolysiloxane, (30 m × 0.250 mm × 0.25 μm film) capillary column. The previously prepared samples were analyzed using identical run parameters for separating the analytes.

2.3.3 NMR spectroscopy. NMR spectra of carnauba wax, pine needle wax, lignin, and the TOFA and octanoic acid esterified lignins were acquired with a 400 MHz (Avance III 400) Bruker instrument equipped with a BBFO probe. The wax samples and lignin derivatives were dissolved in $CDCl_3$, and lignin was dissolved in Dimethyl sulfoxide-d_6 (DMSO-d_6). The $CHCl_3$ (δC, 77.0 ppm; δH, 7.26 ppm) and DMSO (δC, 39.5 ppm; δH, 2.49 ppm) bands were adopted as internal references for chemical shifts, respectively. In ^{1}H spectra, the standard pulse sequence zgig was used with 16 scans, a pulse angle of 90 degrees, an acquisition time of 1 second, and a pulse delay of 5 seconds. Spectral width of 16 ppm was used. The HSQC spectra were run using a Bruker standard pulse sequence hsqcetgpsisp.2. The spectra were collected with 256 increments of 32 scans and using a 2-second pulse delay and 11 ppm spectral width in F2 (^{1}H) dimension with 1024 data points and 215 ppm spectral width in F1 (^{13}C) dimension. Bruker TopSpin 4.1.4 Mac version was used for spectral processing using standard parameters.

2.3.4 Differential scanning calorimetry (DSC). To investigate the thermal properties of starting materials, DSC was measured using TA Instruments DSC 250 equipment. Raw data was exported from TA Universal Analysis and imported to MS Excel from which the DSC curves were created. Sample sizes were 10–16 mg in aluminium hermetic pans with two drilled holes (diameter 0.2 mm). A temperature program used a ramp speed of 10 °C $minute^{-1}$ and nitrogen flow of 50 ml $minute^{-1}$: ramp from −10 °C to 105 °C, isothermal 20 minutes, ramp to 20 °C (annealing cycle), ramp to 190, ramp back to 20 °C

(first heating cycle to remove thermal history), and ramp to 180 °C (second heating cycle used as measurement cycle). The glass transition temperature (T_g) for lignin samples was defined as one-half the change in heat capacity occurring over the transition. T_g was measured from the second heating cycle.

2.4 Nanoparticle preparation

The preparation of lignin nanoparticles (LNPs) commenced in the same manner as previously described.[29,30] In this study, 5 g of kraft lignin was dissolved in 95 g of acetone–water mixture (mass ratio: 3 : 1) for 3 hours. The solution was filtered (paper filters from Whatman, pore size 0.7 μm) to remove undissolved residues. The particles were self-assembled into spherical particles upon rapid pouring of the solution into 350 g of vigorously stirred deionized water. Acetone was removed from the stable colloidal LNP dispersion by using rotary evaporation (40 °C under reduced pressure).

Modified LNPs were produced from esterified lignins with varying degrees of substitution using the same approach as for unmodified kraft lignin. The samples were named as TOFA-LNPs La-LNPs$_{30}$, La-LNPs$_{70}$ and La-LNPs$_{100}$. The solvent was removed from the stable colloidal particle dispersions by evaporation or dialysis using dialysis tubes (SpectraPorR RC Dialysis Membrane, 6–8 kD).

Spruce needle wax particles were produced by adding 0.4 g of wax to 100 ml boiling water and sonicating for 5 minutes at 55% amplitude by using an Ultrasonic Probe Sonifier S-450 (Branson Ultrasonics). The dispersion was cooled in an ice bath immediately after sonication. Afterward, the dispersion was filtered through a glass filter funnel with 100–160 μm nominal maximal pore size. Carnauba wax particles were prepared with a similar procedure as the spruce needle wax particles, detailed information regarding the characterization and particle preparation can be found in ref. 31.

2.5 Characterization of nanoparticles

2.5.1 Hydrodynamic size and ζ-potential. A Malvern Zetasizer Nano (Malvern Instruments, UK) dynamic light scattering device with a dip cell was used to measure the particles' hydrodynamic diameter and electrophoretic mobility. The ζ-potential was calculated from the electrophoretic mobility data by applying the Smoluchowski model. All the measurements were performed in triplicate, and intensity results were reported as an intensity average followed by respective standard deviations.

2.6 Cellulosic substrates

A cellulose nanofibrils (CNF) dispersion was prepared from a never-dried, bleached hardwood kraft pulp. To control the ionic strength and counterion types, the pulp was washed into sodium form prior to disintegration, which was achieved using a high-pressure fluidizer (Microfluidics, M-110Y, Microfluidics Int. Co., Newton, MA) after 6 passes.[32] Freestanding films were prepared through filtration of 100 ml suspension of CNF (0.85 wt% through a Durapore membrane filter with 0.22 μm pore size at 2.5 bar pressure. The films were then dried in a hot press (Fred S. Carver Inc.) at 100 °C for 2 hours with a pressure of 2000 kg cm^{-2} and kept in standard conditions 23 °C and 50% RH) before use.[31]

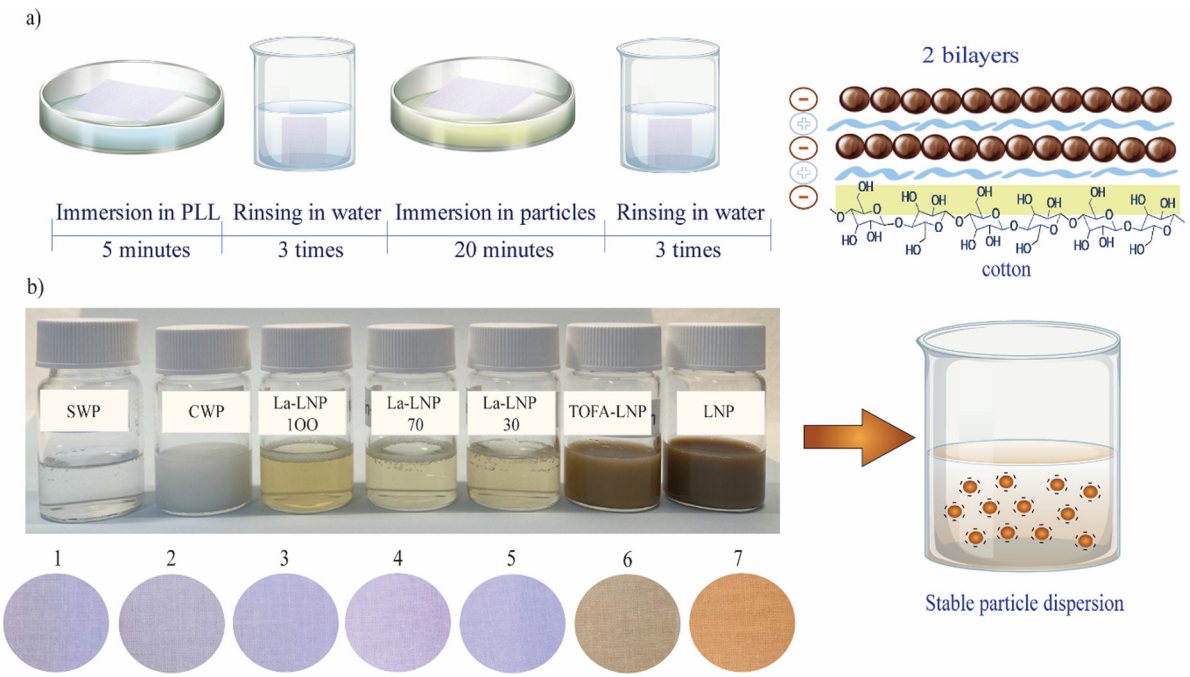

Fig. 1 Illustration of the layer-by-layer procedure for functionalization of the cellulosic substrates. (a) Photographs of aqueous nanoparticle dispersions and cotton fabrics functionalized with the respective NP dispersions. (b) The NP samples from 1–7 are (1) SWPs, (2) CWPs, (3) La-LNPs$_{100}$, (4) La-LNPs$_{70}$, (5) La-LNPs$_{30}$, (6) TOFA-LNPs and, (7) LNPs.

2.7 Textile samples

White lightweight bedsheet fabric of 100% cotton was purchased for the study. The cotton samples were cut into approximately 2 cm × 3 cm pieces and washed with ethanol and water prior to use to remove possible contaminations. The grammage of the textiles was (0.014 ± 0.002) g cm^{-2}, which was an average of three measurements.

2.8 Layer-by-layer coating of freestanding CNF film and cellulose fabric with functional nanoparticles

CNF films and cotton fabric were cut into small strips and soaked in water for a few minutes before the layer-by-layer deposition. Strips were immersed in 0.1 g ml^{-1} solution of poly-L-lysine (PLL) for 5 minutes and thoroughly rinsed with deionized water three times in separate beakers to achieve a uniform deposition of the cationic polyelectrolyte and to remove any unbound or loosely attached molecules from the cellulosic substrate. Next, the strips were immersed in nanoparticle dispersions for 20 minutes, and the substrates were rinsed with water after adsorption. A complete dip-coating cycle provided one bilayer of PLL/particles, which was repeated until 5 bilayers were obtained on CNF films and 2 bilayers on cotton fabrics (Fig. 1). The coated substrates were dried at room temperature between blotting papers under a weight to avoid wrinkles, and then heat treated in an oven for 10 minutes. The oven temperature was specified for each coated sample at 10 °C below T_g of each starting material obtained by differential scanning calorimetry (DSC) (Table 1).

2.9 Characterization of functionalized substrates

Morphology. The surface morphology of the coated cotton fabric was investigated using a field emission scanning electron microscope (FESEM, Zeiss Sigma VP, Germany). A 2 kV accelerated voltage using a secondary electron detector and a working distance of 3–5 mm was used to run the microscope in a vacuum. Prior to imaging, the samples were attached to aluminium SEM stubs with carbon tape, followed by sputter-coating using a Leica Microsystems EM ACE600 coating system. (Leica Microsystems, Wetzlar, Germany) to deposit a thin layer of gold–platinum (5 nm) on the substrate. Fiji ImageJ software (Research Services Branch, NIH, Bethesda, Maryland, USA) was used for image analysis.

Table 1 Differential scanning calorimetry (DSC) results of starting materials: lignin, modified lignin with lauric acid (La-lignin) at three different equivalents (30, 70, and 100), modified lignin with tall oil fatty acid (TOFA-lignin), carnauba wax (CW) and spruce wax (SW)

Sample	T_g (°C)	T_m (°C)
Lignin	133	154
La-lignin30	120	—
La-lignin70	92	—
La-lignin100	50	—
TOFA-lignin	95	130
CW	75	85
SW	55	62

Wetting properties. The interaction between water and coated surfaces was measured by using a Theta Flex optical tensiometer (Biolin Scientific), which utilized a 5 μl water drop to determine the water contact angle (WCA). Four measurements were taken for each sample, and the static contact angle after 20 seconds was reported. Furthermore, the water absorption test was performed using several μl droplets and monitoring the water absorption over time.

Surface roughness. The roughness of the coated freestanding films was measured using atomic force microscopy (AFM) with a Nanoscope V MultiMode scanning probe microscope (Bruker Corporation, Massachusetts, USA). The height images of the coated substrates obtained through AFM were analyzed using Nano Scope Analysis 3 software to calculate the arithmetical mean height (Sa). The Sa analysis was performed on an image with a size of 20 μm^2.

Anti-staining. To evaluate the self-cleaning properties of the coating, two sets of experiments were conducted. In the first experiment set, we evaluated the ability of the coated fabric to repel a colored liquid, specifically methylene blue. We dissolved methylene blue in water and rolled a droplet onto the surface of the fabric, which was tilted at 30 degrees. We then observed the behavior of the liquid on both the coated and pristine fabric. In the second experiment set, we tested the ability of the coated fabric to repel various staining liquids, including red wine, milk, and coffee. Liquid droplets were deposited onto the fabric surface and their behavior was observed.

UV-shielding. The UV-shielding performance of the nanocomposite films was analyzed following the procedure outlined by Kimiaei *et al.* (2022).[33] Rectangular film specimens (3 cm long and 1 cm wide) were cut from samples. The transmittance of the films was measured using Agilent Cary 5000 UV-Vis-NIR Spectrometer (Agilent, CA) across the wavelength range of 200 to 800 nm. The results were reported for each sample as the average value of triplicate measurements.

Reflectance spectroscopy. The color data for the coated fabrics were measured to evaluate the differences in color after treatment. The CIELab coordinates (L^*, a^*, b^*) and reflectance of the dyed samples were recorded using a spectrophotometer (GretagMacbeth Spectrolino). The spectrophotometer was set to D65 illumination and a 10° observer angle. Each sample was measured five times to ensure precision. The color strength (K/S) of the samples was calculated using the Kubelka–Munk equation. This equation relates the reflectance (R) to the absorption (K) and scattering (S) coefficients of the fabric:

$$\frac{K}{S} = \frac{(1-R)^2}{2R}$$

Here, R is the reflectance of the fabric. The measurements were specifically taken at the maximum absorbance.

Bacterial imaging. To study the antibacterial activity of coated samples, lights-off bioluminescent strains were used as described by Jyske *et al.* (2023).[34] An aliquot of 7 ml of bacterial inocula grown overnight was added for every 100 ml of soft agar, Lysogeny agar (LA), (but with 7.5 g l^{-1} (50%) agar

content), supplemented with 10% (v/v) sterile filtered phosphate buffer (PB) (1 M, pH 7.0) and 100 μg ml^{-1} of ampicillin (*E. coli*) and with 5 μg ml^{-1} erythromycin (*S. aureus*) at approximately 50 °C. The soft agar-containing bacteria was mixed gently and rapidly poured over 6-well cell culture plates containing triplicates of 1 cm × 1 cm pieces of the test fabric on a thin layer of LA before the soft agar began to solidify. The plates were then inoculated at 30 °C (*E. coli*) or 37 °C (*S. aureus*) overnight (16 hours) and finally scanned using a SPECTRAL Lago X *in vivo* imaging system (Spectral Instruments Imaging, AZ, United States) with luminescence and image overlay modes. The exposure time of 1 second and small to medium binning (2× to 4×) was used with a field of view (FOV) 25 cm × 25 cm (for 3 Petri plates at once), and an object height of 1.5 cm. Data was then handled using Aura Spectral Instruments Imaging Software version 3.2. Circular whole-well regions of interest (ROIs) were used, and the results were obtained in photons per s per cm per steradian (sr, unit of solid angle). To change the results into more comparable units between bacterial inoculations, the sample result averages from the three plate replicates were divided with a control plate (containing only bacterial inoculation soft agar and no sample) to obtain units of impact factor (IF) and expressed in inhibition percentages (inhibition%).[35] The error bars present the standard deviation between the sample sheets on three plate replicates.

Water vapor transmission rate (WVTR). Water vapor sorption properties of the functionalized cotton fabrics were measured at 25 °C, 65% relative humidity. The test was executed by placing 10 g of dry $CaCl_2$ in a 100 ml glass vial equipped with a sealing screw cap with a hole. To close the glass vial tightly, an aluminium mask with an exchange surface area of 4.9 cm^2 was wrapped around the fabric and placed between the cap and the vial. The mass of the vials was measured in a controlled humidity chamber (RUMED Control 2000, Rubarth Apparate GmbH, Germany) until the change in mass remained consistent within 5% for two successive weightings. For each different sample, three pieces of fabric were measured. The WVTR was determined using the equation below.

$$\mathrm{WVTR} = \frac{\Delta m}{A \times \Delta t}$$

where Δm denotes the increase in mass over time (Δt), and A is the exposed area of the fabrics.

Air permeability. Air permeability was measured using the capillary flow porometer (Porometer 3G micro, USA). In gas permeability mode, the instrument measures the airflow through dry cotton fabrics as a function of a fixed pressure applied. Circular samples (sample area 2.19 cm^2) were cut from each coated fabric. The Frazier AP (mm s^{-1}) was obtained by measuring the airflow rate that passes through the coated samples at the fixed pressure of 125 Pa (12.7 mm H_2O).

Washing fastness. To test the durability of the multifunctional coating on cotton fabrics, real washing conditions were simulated according to international standards (ISO 105-C10:2006). The fabrics were placed in a soap solution with a concentration of 0.5 mg l^{-1} and a pH of 7, with a liquor-to-fabric ratio of 50 : 1. The washing cycle lasted for 30 minutes at 40 °C. After washing, the fabrics were rinsed with distilled water and dried between blotting papers to obtain laundered cotton fabrics.

3. Results and discussion

3.1 Fabrication and characterization of hybrid polyaromatic nanoparticles

The objective of this study was to develop a straightforward, and scalable biobased approach to tune the functionality of cellulosic substrates, such as textiles, by applying a coating of nanoscale particles. For this purpose, we produced hybrid lignin nanoparticles (LNPs) modified with fatty acids with various degrees of substitution and fatty acid carbon chain length. Finally, we compared their properties and performance in textile coatings to unmodified LNPs and NPs derived from natural waxes (spruce and carnauba). FTIR, HSQC NMR, and ^{31}P NMR were used to confirm the successful esterification of lignin, degree of substitution (DS), purity of the modified lignins, and the structural composition of the waxes. The FTIR spectra of unmodified and esterified lignins are illustrated in Fig. 2(a). The successful esterification is reflected by the gradual decrease of the hydroxyl group absorbance (O–H stretching, 3500–3200 cm^{-1}) and the appearance of typical ester C=O group stretching bands at 1760 and 1737 cm^{-1} (non-conjugated phenolic and aliphatic esters, respectively). The increasing absorption bands at 2900–2800 cm^{-1} from the fatty acid alkyl chain $-CH_3$ and $-CH_2$ stretching, moreover verify the incorporation of alkyl chains in the lignin molecules. This derivatization was done to increase the hydrophobicity of the LNPs, since unmodified LNPs are hydrophilic.[30] The esterification reaction linking TOFA and lauric acid (La) to lignin is shown in Fig. 2(c) and (d) respectively. The esterified lignin was subsequently transformed into spherical particles using the solvent exchange self-assembly method.[30] The FTIR spectra of spruce wax and carnauba wax (Fig. 2(b)), display abundant $-CH_3$ and $-CH_2$ group stretching vibrations at wavenumbers of 2910 and 2848 cm^{-1}.

The signal at 1741 cm^{-1} corresponds to the C=O group of the fatty acids and their esters, as expected for natural waxes.[36]

The starting materials, lignin, and the esterified lignins, as well as TOFA and waxes, were further analyzed using 1D and 2D NMR to verify their purity and the success of the modifications (ESI,† Fig. S1a–f). Additionally, ^{31}P NMR was used to determine the degree of substitution (DS) of the three La-lignins and TOFA-lignin (ESI,† Table S1) by quantitative analysis of free OH-groups in each La-Lignin sample. The DS varied from 44% for La-L_{30}, to 60% for La-L_{70}, and 95% for La-L_{100}, respectively. The slight differences in the obtained DS compared to the amount of reagent used in the reaction are most probably due to the post-treatment washing stage. During the post-treatment stage, the product is washed with aqueous ethanol to remove any residual unreacted fatty acid chloride from the product. Especially in La-L_{30} the partially derivatized lower molecular

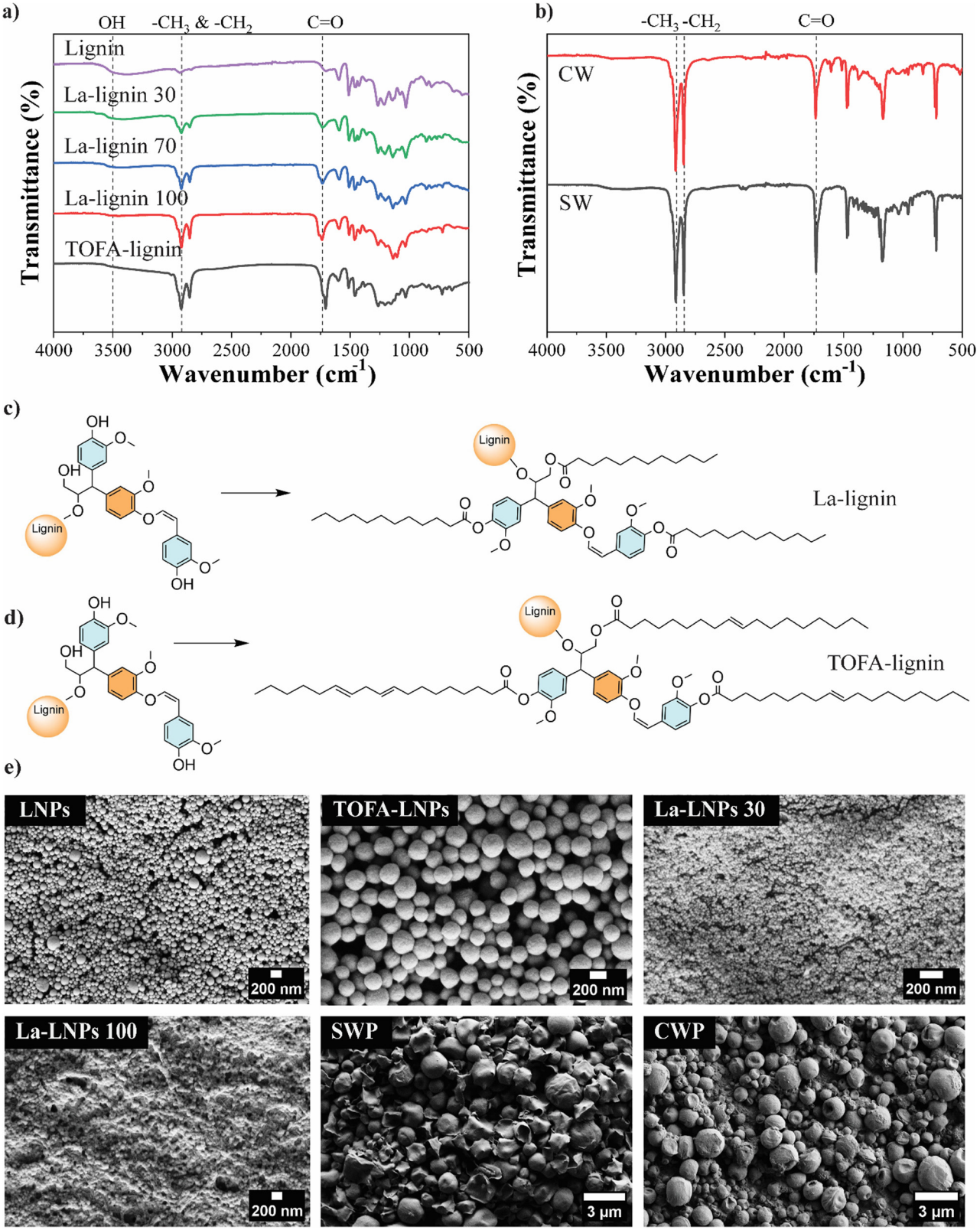

Fig. 2 Chemical characterization of polyaromatic material and morphology of the respective nanoparticle coatings on CNF freestanding films. FTIR spectra of (a) unmodified, esterified lignins, and (b) carnauba and spruce needle waxes. A schematic presentation of lignin esterification by (c) lauric acid chloride and (d) TOFA-chloride. (e) SEM images of CNF freestanding films functionalized with LNPs, TOFA-LNPs, La-LNPs$_{30}$, La-LNPs$_{100}$, CWPs, and SWPs.

weight fraction with higher ethanol–water solubility could be washed out from the product, while the product with a slightly higher degree of substitution remains. The analysis showed that the preferential lignin esterification sites were aliphatic > phenolic > condensed phenolic hydroxyls, where the steric hindrance clearly slowed down the reaction rate and no full esterification was obtained. The DS of the TOFA-lignin was 45%, which could be attributed to the heterogeneous structure of the distilled TOFA and the fact that not all the TOFA acid groups were derivatized when reacted with thionyl chloride. The isolated lignins were used as such for the synthesis of nanoparticles. Seven different types of nanoparticles were prepared using the self-assembly method with unmodified kraft lignin, the esterified lignins La-L_{30}, La-L_{70}, La-L_{100}, TOFA-lignin, and waxes from spruce needle and carnauba. All the components in the hybrid particles were biobased. Softwood lignin and TOFA are byproducts of the chemical pulping process. The primary constituents of TOFA are unsaturated C18-fatty acids, such as oleic and linolenic acids.[18,37] Lauric acid, a saturated medium-chain length (C12) fatty acid, is a major component of coconut oil and palm kernel oil and is naturally found in various plant and animal fats and oils.[38] The particle average hydrodynamic diameters and zeta potentials are shown in Table 2 and their morphologies are shown in Fig. 2(e). All the La-lignins created very small particles, with diameters ranging from 55 to 74 nm. The small size of La-LNPs can be attributed to the lower amount of hydroxyl group leading to less favorable interaction with water, and faster particle formation.[39] The particle size of TOFA-lignin, at 140 nm, exceeded that of unmodified lignin, probably due to the long length of the fatty acid chains C18 and a slightly reduced zeta potential (Table 2). The spruce needle and carnauba waxes formed significantly larger particles than all the lignin-based particles, exhibiting particle diameters of up to (427 ± 173) nm. The zeta potential and size of CWP are in line with previous findings.[21] The zeta potential of the particles varied between −17 mV for TOFA-LNPs to −42 mV for CWPs (Table 2).

This negative zeta potential enables electrostatic repulsion between particles and stable dispersions, as well as electrostatic interaction with cationic PLL during layer-by-layer coating. The La esterification did not alter the carboxylic groups in lignin, hence La-LNPs and unmodified LNPs had similar zeta potentials. The slightly lower zeta potential observed for TOFA-LNPs correlates with the larger particle size together with more steric hindrance during particle formation caused by the long-chain fatty acid esters (ESI,† Table S1) and is in line with previously reported values for TOFA-LNPs.[37]

3.2 Functionalization of cellulosic fabrics with hybrid polyaromatic particles

3.2.1 Surface wettability of the coated fabrics. Cellulosic fabrics are biobased, breathable, and comfortable for the user, however, their tendency to absorb moisture restricts their use in more demanding applications, such as high-performance outdoor apparel, industrial workwear, medical textiles, and athletic performance wear.[40] To investigate how the different particulate coatings from unmodified kraft lignin, esterified lignins, and waxes affected the wetting properties of cellulosic fabrics static water contact angles (WCA) were measured from 0 to 20 seconds and the value at 20 seconds is given in Fig. 3(a). The reference (uncoated) cotton fabric had a contact angle of (43 ± 15)° during the first 20 seconds and absorbed the water droplet in less than one minute as expected due to the abundance of hydroxyl groups in cellulose. Fabrics coated with unmodified LNPs absorbed the water in less than 20 seconds due to the hydrophilicity of unmodified LNPs. In contrast, coatings based on hybrid lignin nanoparticles effectively hydrophobized the fabrics, increasing the WCA of La-LNPs samples with varying fatty acid-to-lignin ratio, to around 130°. There was no significant difference between the LNPs with different DS of esterification, good hydrophobicity was obtained even for the sample with the lowest DS (La-$LNPs_{30}$). Surprisingly, the WCA for fabrics coated with TOFA-LNPs was only 71°. Despite the seemingly low coverage of both spruce needle and carnauba wax NPs (Fig. 3(c)) the WCA on the fabrics coated with wax NPs significantly increased to almost 150°. Partial coverage has been shown to be sufficient to induce significant changes in wetting properties and similar results have been found for cellulose fabric coated with CWPs[41] although SWPs have not been studied previously.

Table 2 Hydrodynamic diameter, dispersity, and zeta potential of the nanoparticles

Sample	Size (nm)	Dispersity	Zeta potential (mV)	pH
LNPs	119 ± 1	0.12	−30 ± 3	3.8
TOFA-LNPs	139 ± 9	0.14	−17 ± 1	4.3
La-$LNPs_{30}$	55 ± 2	0.41	−27 ± 1	4.1
La-$LNPs_{70}$	47 ± 2	0.47	−34 ± 1	4.3
La-$LNPs_{100}$	74 ± 1	0.11	−35 ± 4	4.1
CWP	427 ± 173	0.15	−42 ± 3	6.3
SWP	393 ± 9	0.58	−29 ± 2	4.8

To further improve the hydrophobicity of the coated fabrics, a thermal annealing step was applied to each sample for 10 minutes. Thermal annealing could additionally improve the adhesion between the particles and the cellulosic substrate.[42] The annealing temperature was selected based on DSC results (Table 1, and ESI,† Fig. S7). For each system, temperatures 10 °C below T_g were chosen. This choice provided enough energy for the reorientation of different moieties without fully melting the particles. As a result, more hydrophobic moieties were brought closer to the air interface, increasing the surface hydrophobicity without sacrificing the roughness of the surface.[43]

The most significant increase in WCA after thermal annealing was observed for the TOFA-LNP coating, which increased from 71° to 141°. We speculate that the abundance of carboxylic functional groups in TOFA, observed in ^{31}P NMR (ESI,† Table S1), initially contributes to the low contact angle of the TOFA-LNP coating. However, during heat treatment, owing to the long hydrocarbon chain (C18) and the low melting point of TOFA, it appears to migrate more readily to the nanoparticle surface during annealing, potentially also exposing more of the hydrophobic hydrocarbon

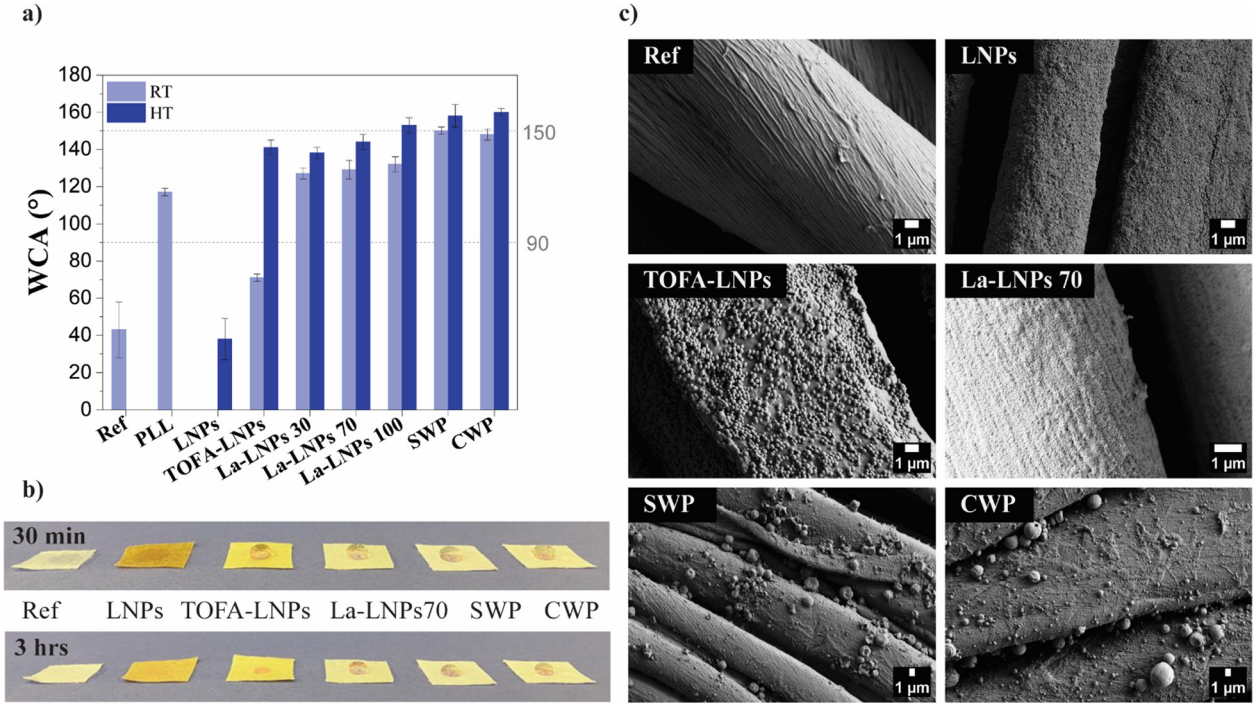

Fig. 3 Wetting properties and morphology of layer-by-layer coated and uncoated cotton fabrics. Ref is the uncoated cotton fabric and PLL is the fabric coated only with the cationic PLL. Other samples were coated with LNPs, TOFA-LNPs, La-LNPs$_{30}$, La-LNPs$_{70}$, La-LNPs$_{100}$, SWPs, and CWPs layers. (a) Static WCA at 20 seconds exposure using 5 μl water droplets. NP coated samples were measured both at RT and after annealing (HT), the HT temperature was specified for each coated sample at 10 °C below T_g (Table 1), ranging from 45 °C for SW to 120 °C for lignin. (b) Photographs of water droplets on the cotton fabric and annealed coated cotton fabric 30 minutes and 3 hours after exposure, showing possible absorption or spreading. (c) SEM images of cotton fabric before and after coating. Pristine fabric, and fabric coated with LNPs, TOFA-LNPs, La-LNPs$_{100}$, SWPs, and CWPs.

chain, substantially increasing the contact angle. After the heat treatment, the coated samples with La-LNPs$_{100}$, spruce needle wax, and carnauba wax all reached superhydrophobicity with WCA of (153 ± 4)°, (158 ± 6)°, and (160 ± 2)°, respectively. Previously, superhydrophobic coatings have mainly been achieved using synthetic polymers like polydimethylsiloxane or perfluorinated compounds[44,45] and less often by using biobased coatings. A few positive exceptions are *e.g.*, the work of Luo *et al.* (2021)[46] demonstrating a WCA of 153.3° on cotton fabric coated with tannic acid, borax, and poly-dopamine and Forsman *et al.* (2017) using CWPs.[31] The small water droplets of 5 μl used for WCA measurements evaporated quickly, and therefore, to assess the long-term water repellency and degree of water absorption, macroscopic water droplets of several ml were deposited onto both pristine and functionalized fabrics and imaged at 0.5, 1, 1.5 and 3 hours, respectively (Fig. 3(b) and ESI,† Fig. S9). Notably, the samples coated with La-LNPs$_{70}$ and wax NPs exhibited the most impressive water droplet stability. The droplets remained stable for more than 3 hours and showed no sign of absorption or spreading. The sample coated with TOFA-LNPs also showed good water droplet stability, although the droplets started to absorb after one hour. This excellent water repellency for several hours is in drastic contrast to results for non-particulate lignin TOFA ester coatings that showed stable water droplets for only 2 minutes and a contact angle of 80°.[47] Another study reported that a four-layer coating using the phenolic compound, benzoxazine, achieved a contact angle of 120°.[48] This comparison to previous literature clearly demonstrates the advantage of using particulate coatings compared to smooth films.

3.2.2 Morphology and surface roughness. SEM and AFM imaging were combined to correlate the observed wetting and anti-staining properties with the morphology of the samples. SEM microscopy shows that the pristine cotton fabric appears rough at a macroscopic level due to its woven structure. This macroscopic structure is also retained for all coated fabrics. The surface of each fiber in the pure cotton material was initially smooth with only minor structures visible, while functionalization with a particulate coating led to a granular surface structure. Deposition of two bilayers of PLL/particles resulted in complete, uniform, and homogeneous coverage of the fabric samples with lignin-based particles and satisfactory coverage of wax-based particles (Fig. 3(c)).

We chose the LbL strategy and PLL as the cationic layer for attaching the hybrid particles onto cellulosic textiles due to previous positive experiences with this approach. QCM-D studies have shown that PLL adsorbs onto cellulose[31] and that both unmodified LNPs[30] and CWPs[31] adsorbs onto PLL. These studies suggested that the adsorption was mainly driven by the entropy gain due to the release of counterions and bound water from both the substrate and the particles upon adsorption. We assume a similar binding mechanism also for the La-LNPs and SWPs that hasn't been studied previously.

SEM micrographs of the coated samples after heat treatment can be found in the ESI† (Fig. S8). We assume that the

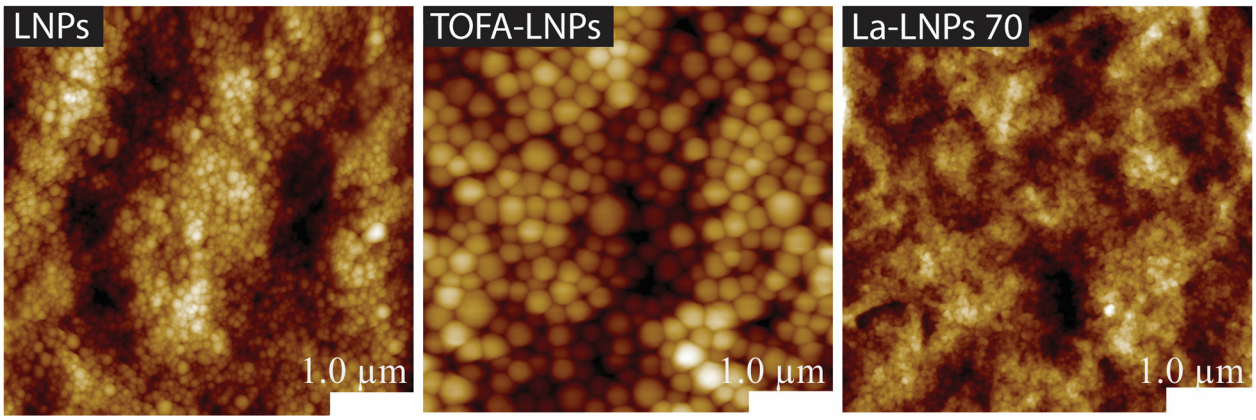

Fig. 4 AFM height images of functionalized freestanding films with LNP, TOFA-LNP, and La-LNP$_{70}$ coatings.

macroscopic roughness of the fabrics was the same in all samples.

Therefore, we used AFM to investigate the relationship between particle size, distribution, and micro and nanoscale roughness of coatings on CNF freestanding films (Fig. 4 and Table 3). Thick coatings can fill all voids of the fabric, leading to a decrease in surface roughness. However, the coatings applied here were thin enough that this effect should be negligible. The particle distribution on the freestanding CNF films was uniform, and there was no evidence of aggregation (Fig. 4). The CNF surfaces coated with a good nanoparticle's coverage, such as the La-LNP coated CNF, exhibited lower Sa values compared to films with a larger NPs size range, such as the CWP coated CNF. This is because the small La-LNPs particles could produce an even continuous coating on the surface. Comparing the WCA of the coatings on a smooth CNF film (Table 3) with the WCA on cotton fabrics (Fig. 3) it is evident that the macroscopic roughness of cotton is essential for the observed superhydrophobicity.

The clearly rougher CWP and SWP coatings resulted in qualitatively similar WCA as the LNP-based coatings with smaller Sa. This indicated that on smooth substrates, the surface chemistry of the compounds dominates the wetting properties and the effect of nanoscaled roughness was not evident. These findings align with the observations by Henn *et al.* (2021), who noted that thicker LNP coating layers on wood led to reduced surface roughness due to closely packed particles.[24] Similarly, Dong *et al.* (2010) demonstrated that the roughness of the surfaces initially increased in the presence of particles on the CNF film and then decreased with an improvement in surface coverage.[41]

Table 3 The effect of different coating on the surface roughness of CNF film presented arithmetical mean height (Sa), measured five times for each sample with size of 20 μm2 and WCA of coated CNF at room temperature (RT) and after heat treatment (HT)

Sample	Sa (nm) RT	WCA (°) RT	WCA (°) HT
LNPs	97 ± 10	56 ± 3	72 ± 1
TOFA-LNPs	89 ± 11	42 ± 8	118 ± 3
La-LNPs$_{30}$	92 ± 14	92 ± 1	102 ± 2
La-LNPs$_{70}$	77 ± 6	110 ± 1	105 ± 4
La-LNPs$_{100}$	95 ± 12	118 ± 2	106 ± 1
SWP	245 ± 33	105 ± 3	105 ± 4
CWP	138 ± 50	114 ± 6	117 ± 6
CNF (ref)	82 ± 4	—	—

3.2.3 Anti-staining properties. The ability to resist staining allows garments to maintain a clean appearance and reduces the need for frequent washing leading to more efficient management of multifunctional fabrics.[49] Inspired by the WCA values above 150° and excellent water repellency, we investigated the anti-staining properties of coated fabrics by dropping an aqueous solution of methylene blue on coated fabric specimens at tilting angle of 30°. The Methylene blue droplets remained on the surface of pristine cotton fabric and fabrics coated with unmodified LNPs. In contrast, no methylene blue stains were left on the samples coated with modified lignin and wax NPs (Fig. 5(a)–(f)) (Fig. S10, S11 and Video in ESI†). Coatings with a combination of low surface energy and high roughness can induce anti-staining properties, where water droplets roll off the coated surface and simultaneously remove dirt (Fig. 5(g)). This is often due to air pockets formed between the particles, leading to the surface not being fully wet, as described by the Cassie–Baxter equation (ESI,† eqn (S1)).[50] To classify a surface as self-cleaning the roll-off angle coatings should be less than 10°. In our case, the water droplets did not roll off easily at tilting angles below 30°. Additionally, we tested the stain resistance against typical food stains by using milk, coffee, and wine. All liquids formed stable droplets with high contact angles on La-LNPs$_{70}$ coated cotton (Fig. 5(i)), while they were immediately absorbed by the reference fabric (Fig. 5(j)). The high WCA (>150°) and excellent anti-staining properties of La-LNPs$_{70}$ and wax NP coated cotton fabrics suggest that both the roughness and the low surface energy of the coatings are important.

3.2.4 Spectrophotometric measurement. Currently, skin cancer ranks among the most widespread forms of cancer globally. Therefore, enhancing the ability of textiles to provide protection against UV radiation is gaining interest, particularly for garments designed for children, sports, and work.[51] Cellulosic fabrics have a low UV protective factor due to a lack of UV

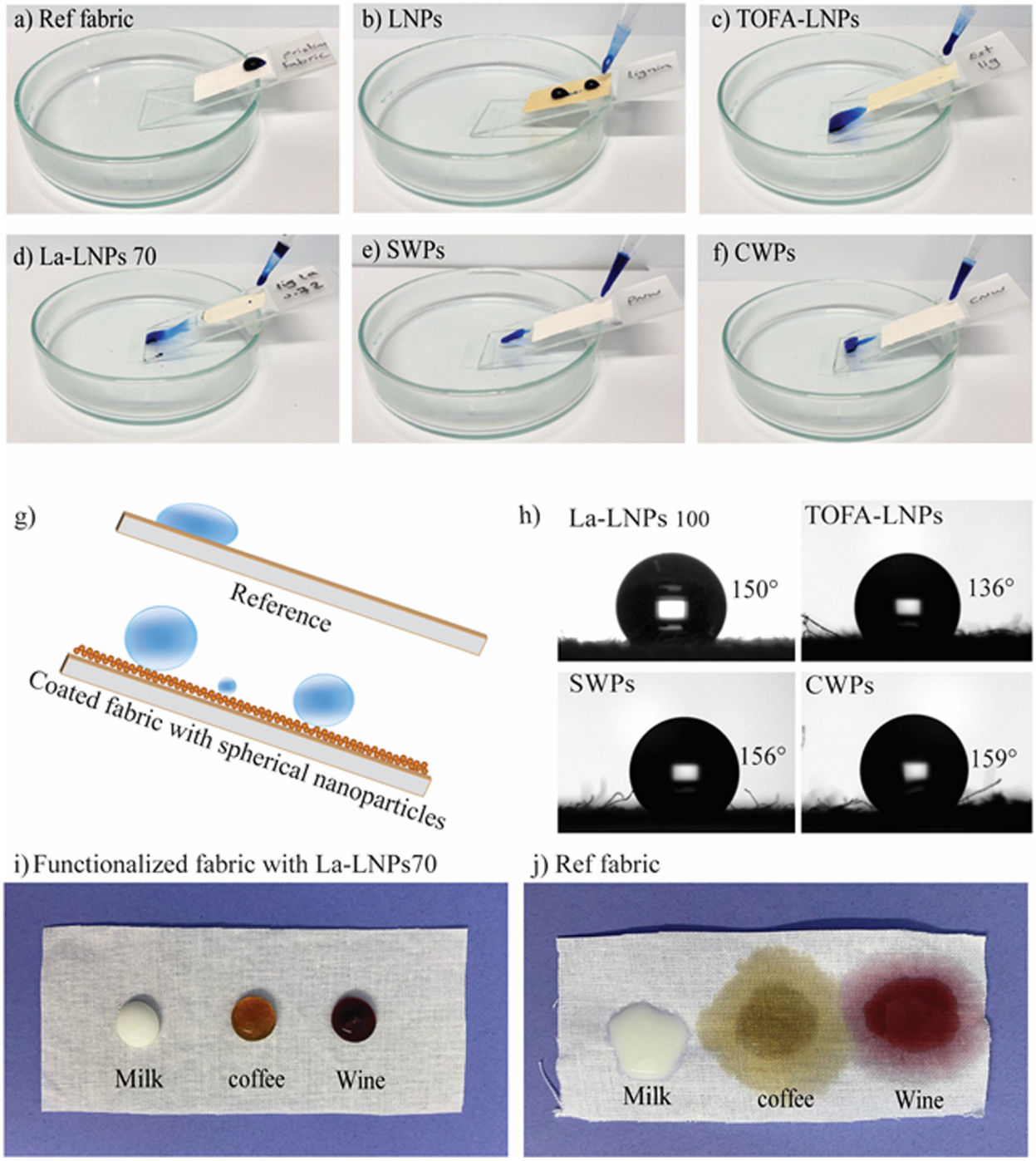

Fig. 5 Anti-staining properties of NP coated fabrics. Photographs of deposited methylene blue solution drop on a 30-degree angle tilted (a) reference fabric, (b) LNPs, (c) TOFA-LNPs, (d) La-LNPs$_{70}$ (e) SWPs, (f) CWPs coated fabrics. (b) Schematic illustration of water droplets' behaviour on a tilted smooth or particle coated surface. (h) Photographs of the water droplet profile on top of coated cotton fabric acquired at 20 s during WCA measurements. (i) Photographs of milk, coffee, and wine droplets on the La-LNPs$_{70}$ coated and (j) the reference uncoated cotton fabric.

adsorbing structures. However, adding a layer of functional nanomaterial is attractive to protect both the fabric and the user. To evaluate the UV-blocking potential of the biobased coatings on cellulosic materials, CNF freestanding films were functionalized using 5 bilayers of the NPs. The untreated CNF freestanding film exhibited up to 90% UV-blocking at short wavelengths in the UV-C region due to the physical thickness of the film while its light-blocking capacity reduced gradually with increasing wavelengths at UV-B and UV-A regions, showing light transmittance of 25% at a wavelength of 350 nm (Fig. 6(a)). In contrast, all coated samples demonstrated increased suppression of light transmittance in the UV-A, UV-B, and UV-C regions. The transmittance of the coated films showed a higher blocking percentage for UV-B compared to UV-A. The film coated with

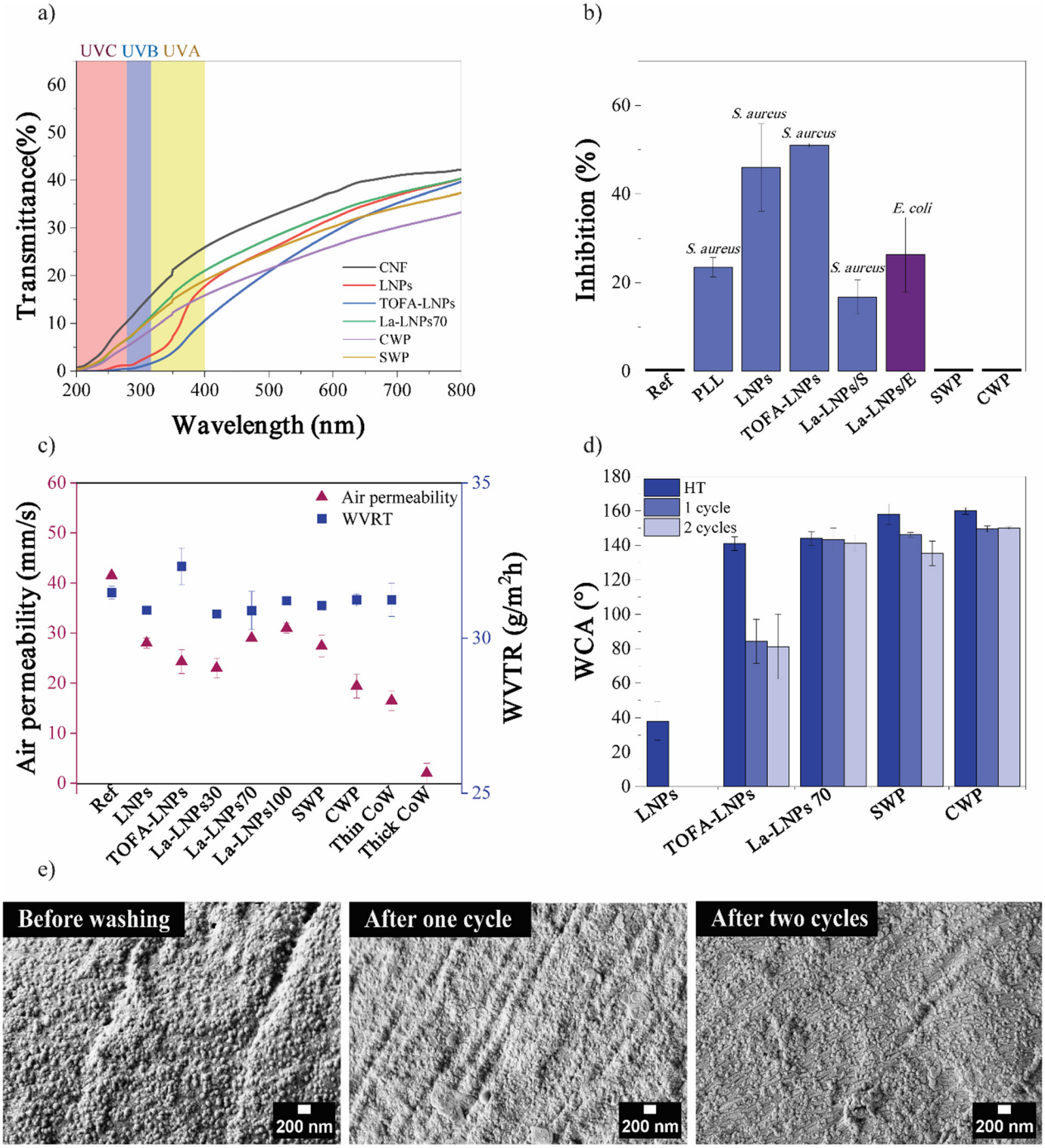

Fig. 6 (a) UV-vis light transmittance spectra of coated and uncoated CNF films. (b) The antibacterial effect of the nanoparticle coatings involving the inhibition of bacterial growth against *S. aureus* and *E. coli* on cotton fabric. (c) Textile breathability of coated cotton fabric as a function of WVTR (g m^{-2} h^{-1}) and air permeability (mm s^{-1}). Washing fastness of the coatings on cotton fabrics. (d) Changes in WCA (°) after one and two cycles of washing. (e) SEM images of the La-$LNPs_{70}$ coated fabric before washing and after one and two cycles of washing.

LNPs and TOFA-LNPs demonstrated almost complete absorption in the UV-B (280–315 nm) region and strong UV absorption in the UV-A (315–400 nm) region due to the effective absorption of UV radiation of the conjugated structures present in lignin. The kraft lignin contains a high amount of aromatic UV chromophore groups, such as methoxy-substituted phenoxy groups with some conjugated double bonds, carbonyl functional groups, and quinone structures enabling broad-spectrum UV light absorption within the range between 250 and 400 nm.[52] The presence of conjugated double bonds within TOFA molecules in TOFA-LNPs grants them an increased ability to absorb UV light within the 200–400 nm wavelength range.[53] In contrast, the La-$LNPs_{70}$ coating demonstrated slightly lower UV-blocking capacity, which may be linked both to the diminished presence of phenolic

hydroxyl groups in the modified lignin and the incorporation of a high number of saturated fatty acids esters per weight lignin. As a result, La-lignin70 samples had only 40% of the original phenolic hydroxyl content of unmodified lignin (ESI,† Table S1). Previously, smaller lignin nanoparticle dispersion (<100 nm in size) exhibited higher UV-light absorbance in the 290–360 nm wavelength range compared to larger particles.[54]

We observed that in addition to the particle size, the chemical composition of particles significantly influences their UV-blocking capabilities. Specifically, the presence of lauric acid in lignin nanoparticles was found to diminish the UV-blocking efficacy of esterified lignin particles. Additionally, this chemical component had an impact on the color of the nanoparticle dispersion, resulting in a brighter appearance compared to the unmodified counterpart and consequently also reduction of the physical barrier as well (Fig. 1(b)).

To verify the effect of surface functionalization with nanoparticles on the color shading of white cotton, color coordinates (L^*, a^*, b^*, and C^*) and color strength (K/S) of coated fabrics were measured. The data are presented in Table 4. Surface functionalization of white cotton fabric with polyaromatic nanoparticles resulted in an increase in both a^* and b^* values, indicating a shift towards a reddish-yellow color. This shift was most significant for LNP followed by TOFA-LNP. The same was observed in the photographs of coated samples (Fig. 1(b)). Unmodified LNPs and TOFA-LNPs changed the visual appearance of the fabric from white in native cotton to beige upon coating. However, the La-LNP, SWP, and CWP coatings did not result in a visual color change. Hence, especially La-LNPs are very interesting for textile modification since they provide multifunctionality without changing the color of the sample.

3.2.5 Anti-bacterial properties of the nanoparticle coated fabrics. Antimicrobial textiles are crucial in maintaining hygiene, particularly in healthcare settings. They offer a sustainable option for single-use materials while reducing textile waste. Furthermore, they are becoming popular in sportswear by preventing the growth of bacteria and unpleasant odors, resulting in improved performance and comfort.[55] Since we aimed to develop multifunctional biobased coatings, we investigated the microbial inhibition of coated fabric against two common pathogens: the Gram-positive bacterium *Staphylococcus aureus* (*S. aureus* RN4220 + pAT19) and the Gram-negative bacterium *Escherichia coli* (*E. coli* K12 + pcGLS11). These bacteria account for a significant proportion of surgical site infections (SSIs) that require hospitalization. According to Abdullah *et al.* (2021), *S. aureus* and *E. coli* are responsible for 18.8% and 17.3% of such infections, respectively.[56] The antibacterial effect of the particle coated fabric samples is expressed as the average bacterial growth inhibition percentages ± standard deviation between three replicates (Fig. 6(b)), and images of luminescent bacteria plates are shown in ESI,† Fig. S12. The results show that LNPs and TOFA-LNPs exhibited the highest activity against *S. aureus*, resulting in growth inhibition of 46 ± 10% and 51 ± 1%, respectively. The sample coated with only PLL had weaker antimicrobial activity than TOFA-LNPs and unmodified LNPs against *S. aureus* but slightly higher than La-LNPs. Interestingly, La-LNPs demonstrated some activity against both *S. aureus* and *E. coli*, resulting in growth inhibition of 17 ± 4% and 26 ± 8%, respectively, for the different bacterial strains. The lower inhibition of these particles may be attributed to their small particle size (between 50–70 nm) and lower layer thickness, which has previously been observed to impact the antibacterial activity of lignin particles.[37,57] Jyske *et al.* (2023) emphasized that the inclusion of tannin-rich bark extract in fiber networks introduced an inhibition rate of approximately 30%, which was highly dependent on the thickness of the fiber network.[34] However, our antibacterial coating, derived from LNPs and TOFA-LNPs, consistently outperformed the previously reported values for natural components in the literature in terms of inhibition percentages against *S. aureus*. Our study reports inhibition percentages, differing from the common inhibition zone measurements (in. mm) in existing literature, complicating more direct comparisons with prior research. We employed an advanced antibacterial method that combines both visual assessment and numerical antibacterial calculation *via* photon counting which enabled us to see the antibacterial effects with even extremely low concentrations of the active substances, demonstrating a higher accuracy compared to conventional methods. Lignin is believed to possess antimicrobial properties mainly due to its phenolic compounds. These compounds, which have a double bond of α and β carbon linked by a methyl group in the γ position, can disrupt bacterial cell membranes, leading to the release of biological components in cells.[58] Similarly, free fatty acids and their monoglyceride derivatives have known antimicrobial properties.[59] In particular, La, an unsaturated fatty acid, can inhibit bacterial growth by disrupting the cell membrane and inducing the production of reactive oxygen species.[60] Previous studies on the antibacterial activity of TOFA-LNP dispersion, also found that the bacterial inhibition of TOFA-LNPs was higher than that of unmodified LNPs (31 ± 6% and 23 ± 1%, respectively).[37] Moreover, the inhibitory effect of unsaturated fatty acids was found to be greater than that of saturated fatty acids, which is consistent with other studies.[61] The results of this study suggest that lignin fatty acid nanoparticles have promising antimicrobial properties that could be utilized in the development of novel coatings for use on textiles to prevent SSIs caused by *S. aureus* and *E. coli*.

3.2.6 Breathability. Good breathability is important for functional textiles. Clothing with good breathability is comfortable for the wearer because it allows moisture generated by the human body to be released to the surface of the fabric.[62–64]

Table 4 Color measurement results for reference cotton and coated fabrics

Sample	Color name	L^*	a^*	b^*	K/S
Reference cotton	White	92.9	0.04	−0,5	0.02
LNPs	Beige	65.8	11.3	19.1	0.58
TOFA-LNPs	Beige	80.7	3.8	19.6	0.13
La-LNPs70	White	91.5	−0.01	3.8	0.02
SWPs	White	93.3	−0.08	1.1	0.02
CWPs	White	92.9	0.1	2.3	0.02

Herein, we evaluated the effect of the biobased coatings on the breathability of fabrics using two complementary measurements, water vapor transmission rate (WVTR) and air permeability. In general, waterproof microporous textiles have pores that are smaller than raindrops but larger than water vapor molecules providing resistance to the penetration of liquid water while still allowing water vapor to pass through. The WVTR values of the coated fabrics were similar to those of pristine cotton (Fig. 6(c)), indicating that these multifunctional nanoparticle coatings maintained the high water vapor permeability of the material.

Cotton fabric can be considered as a pseudo-2D porous material, characterized by a complex pore structure at various scales. On a microscopic level, there are pores between the warp and weft yarns, typically larger than 5 μm. At a smaller scale, submicron pores are present between the individual fibers within a yarn, ranging in size from 100 nm to 10 μm. Additionally, the fibers themselves contain even smaller nanopores, with diameters of less than 100 nm, owing to the inherent porous nature of cotton fibers.[65]

Based on the SEM images (Fig. 3(c)), the pores between the yarns which were initially micron-sized, became slightly narrower shifting to the submicron range after coating. It is possible that the nanoparticles partially clog the nanopores within the individual fibers slightly reducing the air permeability, while the air can still flow between fibers. The CWP coating exhibited the lowest air permeability. Due to the variation in particle size with both small and large particles present, it probably partially blocked the nanosized pores, but the fabric was still considered breathable because of the partly open submicron pores. In contrast to the WVTR, the coating affected the air permeability. The air permeability decreased around 30% from 41 mm s^{-1} for pure cotton fabric to a range of 23 to 31 mm s^{-1} for the coated samples (Fig. 6(c)). In a study by Maksoud *et al.* (2017), a commercial waterproof breathable fabric showed an air permeability of 8 mm s^{-1} and a WVTR of 36 g m^{-2} h^{-1}.[66]

At first sight, the air and water vapor permeability seem to be in conflict. However, considering the different mechanisms the results are logical. Air permeability occurs in convection conditions, where a large surface area is advantageous for air permeability. In contrast, since water vapor permeability occurs under free convection conditions, it is determined not only by porosity and pore diameter but also by the interaction between pore surface and water, leading to capillary forces.[67,68]

In the uncoated cellulosic fabric, water can form hydrogen bonds with hydrophilic hydroxyl groups on the cellulose molecules slowing down the water vapor transport. The coating with the polyaromatic NPs renders the cotton fabric hydrophobic decreasing the attraction between water and fabric. Therefore, the relatively fast movement of water vapor through the coated fabrics is explained by the weak attraction between the water molecules and NP coated fabric, as well as the hydrogen bonds formed between the water molecules.[65]

The capillary effect also plays an important role in the water vapor transmission through the fabric. The spaces between fibers form capillaries, and the smaller the spaces between fibers, the better the textile's ability to remove moisture. The size, volume, and number of capillary gaps within the fiber bundle determine the wicking effectiveness of the yarn.[65,68] For comparison, cotton fabrics were treated with commercial Greenland wax (referred to as CoW) using both thin and thick coatings of the wax. The results revealed that a thin coating allowed for breathability but exhibited poor water repellency (WCA $(54 \pm 3)^\circ$), whereas a thick layer of this commercial coating blocked all the pores and dropped the breathability while demonstrating good water repellency (WCA $(114 \pm 2)^\circ$). It is worth highlighting that increased thickness in coating layers may hinder air permeability which underscores the importance of opting for thinner layers to achieve a balance between water repellency and breathability.[69] In addition, this result is consistent with previous studies reporting that the WVTR value did not change after cotton was treated with a waterproofing finish. This is due to the reduced interaction between the surfaces of the textiles and water molecules, as well as the increased capillary effect of the deep grooves generated between the fibers.[65]

3.3 Stability of the coating – wash fastness

The wash fastness of the coatings was evaluated using static WCA values and SEM (Fig. 6(d), (e), and (ESI,† Fig. S13)). The WCA values of the La-LNP_{70} coated cotton fabric only decreased from $(144 \pm 4)^\circ$ (after heat treatment) to $(141 \pm 5)^\circ$ after 2 washing cycles. Based on the wash fastness test La-LNP_{70} coated cotton fabrics exhibited high stability during washing. Even after one or two washings, the coating showed considerable resistance to detachment from the fabric, shown by the presence of particles on the fabric after washing in SEM micrographs (Fig. 6(e)). The exceptional wash fastness of the coating can be attributed to the strong bonding between the La-LNPs and the PLL coated cotton fabric. This is a promising result, as it suggests that the coating has the potential to retain its functional properties after repeated use and washing. Our contribution to wash fastness data addresses a gap in prior wax coating studies.[25] The presence of La in the coating contributed to its water-repellent properties, which could help protect the underlying cotton fabric from damage during the washing process.

As a quick test for scalability, the application of La-LNP_{100} coating to the fabric through the spray method was tested. Following the application of a single bilayer of this coating, a notable enhancement in the contact angle to $(135 \pm 2)^\circ$ was observed (ESI,† Fig. S14). Additionally, SEM analysis confirmed the successful attachment of particles to the fabric's surface (ESI,† Fig. S14). This spray application method offers a convenient and user-friendly approach for applying coatings to various textiles, including outdoor winter clothing, outdoor furniture, and other fabrics requiring diverse functionalities and breathability.

4 Conclusion

We have successfully developed multifunctional coatings using biobased materials derived from wood and plant components.

The utilization of aromatic hybrid lignin nanoparticles and wax particles facilitated the fabrication of a 100% biobased coating on cotton fabric through a layer-by-layer deposition technique. *Via* systematic comparison of a range of different polyaromatic nanoparticles, we found that the incorporation of fatty acids into the lignin particles improved the hydrophobicity of the coating, and the inclusion of phenolic structures added both antibacterial and UV-blocking properties to the cellulosic fibers, while wax particle coatings lacked these properties. Furthermore, our hydrophobic coating demonstrated robustness, maintaining its water droplet-repelling characteristics for several hours, a feature not previously indicated in other studies. Additionally, the use of aqueous particle dispersions made spreading of the coating easy, providing excellent surface coverage, while maintaining the breathability of the fabric. Overall, the results demonstrate potential of utilizing biobased materials to produce multifunctional coatings for textiles. These coatings offer high potential for various textile applications: providing water and stain repellency for outdoor clothing, ensuring safety and hygiene for industrial workwear, promoting comfort and bacteria prevention for medical textiles, and offering UV protection and breathability for athletic performance wear. By systematically coupling the performance to the chemistry and morphology of the particles we envision that these findings can be used to further develop sustainable and eco-friendly coatings for various applications in the textile industry.

Author contributions

The conceptualization and design of the coating fabrication experiments were led by SB and PN. SB tested the coating properties and analyzed data regarding SEM, AFM, WCA, DSC, and FTIR, in addition to evaluating breathability and wash fastness. EK conducted UV testing. Antibacterial analysis was carried out by JT, while NMR and GC–MS analyses and their interpretation were conducted by PN. NK prepared TOFA-LNP. RK conducted GC–MS for needle wax. KK produced needle wax. PN provided scientific guidance and support throughout the writing process. MÖ reviewed and revised the manuscript and provided scientific guidance.

Data availability

The data that support the findings of this study are available on request from the corresponding author. The data are not publicly available due to privacy or ethical restrictions.

Conflicts of interest

The authors declare no conflict of interest.

Acknowledgements

This work was funded through the Aalto University Bioinnovation Center, which was established by a grant of the Jane and Aatos Erkko Foundation (SB) and the European Union – NextGenerationEU instrument and by the Academy of Finland under grant number 348870 (PN) and 349052 (RK, JT, KK). The authors thank Ulla Jauhiainen for the proficient technical assistance with the bacterial tests at the Luke laboratories. The authors thank Dr Heidi Henrickson for proofreading the manuscript and helping to improve its overall quality.

References

1 J. Liu, S. Qiu, P. Qi, J. Sun, H. Li and X. Gu, *et al.*, Constructing a Fully Biobased Coating to Improve the Flame Retardancy, Antibacterial Properties, and UV Resistance of Polyamide 6 Fabrics, *ACS Appl. Eng. Mater.*, 2023, **1**(1), 268–277, DOI: **10.1021/acsaenm.2c00061**.

2 L. Zhu, X. Ding, X. Wu, Z. Yan, S. Lei and Y. Si, Innovative and Sustainable Multifunctional Finishing Method for Textile Materials by Applying Engineered Water Nanostructures, *ACS Sustainable Chem. Eng.*, 2020, **8**(39), 14833–14844, DOI: **10.1021/acssuschemeng.0c04252**.

3 H. E. Emam, M. El-Shahat, M. S. Hasanin and H. B. Ahmed, Potential military cotton textiles composed of carbon quantum dots clustered from 4-(2,4-dichlorophenyl)-6-oxo-2-thioxohexahydropyrimidine-5-carbonitrile, *Cellulose*, 2021, **28**, 9991–10011, DOI: **10.1007/s10570-021-04147-4**.

4 B. Abdi, A. Tarhini, H. Baniasadi and A. R. Tehrani-Bagha, Developing Graphene-based Conductive Textiles Using Different Coating Methods, *Adv. Mater. Technol.*, 2024, **9**, 2301492, DOI: **10.1002/admt.202301492**.

5 B. Szadkowski, M. Śliwka-Kaszyńska and A. Marzec, Bioactive and biodegradable cotton fabrics produced *via* synergic effect of plant extracts and essential oils in chitosan coating system, *Sci. Rep.*, 2024, **14**, 8530, DOI: **10.1038/s41598-024-59105-4**.

6 G. Xia, X. Bian, Y. Wang, Y. Lam, Y. Zhao and S. Fan, *et al.*, Janus outdoor protective clothing with unidirectional moisture transfer, antibacterial, and mosquito repellent properties, *Chem. Eng. J.*, 2024, **490**, 151826, DOI: **10.1016/j.cej.2024.151826**.

7 H. E. Emam, S. Zaghloul, H. B. Ahmed, H. E. Emam, S. Zaghloul and H. B. Ahmed, Full ultraviolet shielding potency of highly durable cotton *via* self- implantation of palladium nanoclusters, *Cellulose*, 2022, **29**, 4787–4804, DOI: **10.1007/s10570-022-04567-w**.

8 H. E. Emam, M. H. El-Rafie and M. Rehan, Functionalization of Unbleached Flax Fibers by Direct Integration of Nano-silver through Internal and External Reduction, *Fibers Polym.*, 2021, **22**(11), 3014–3024.

9 M. A. Shah, B. M. Pirzada, G. Price, A. L. Shibiru and A. Qurashi, Applications of nanotechnology in smart textile industry: A critical review, *J. Adv. Res.*, 2022, **38**, 55–75.

10 J. Zhao, W. Zhu, X. Wang, L. Liu, J. Yu and B. Ding, Fluorine-Free Waterborne Coating for Environmentally Friendly, Robustly Water-Resistant, and Highly Breathable Fibrous Textiles, *ACS Nano*, 2020, **14**(1), 1045–1054, DOI: **10.1021/acsnano.9b08595**.

11 Z. Long, L. Yuan, J. Chen, L. Luo, C. Shi and C. Wu, *et al.*, A Durable Fluorine-Free MOF-Based Self-Cleaning Superhydrophobic Cotton Fabric for Oil-Water Separation, *Adv. Mater. Interfaces*, 2022, **9**(13), 1–10.

12 W. Liu, R. Zhang, G. Duan, L. Zhang, Y. Li and L. Yang, Bio-inspired and Multifunctional Polyphenol-Coated Textiles, *Adv. Fiber Mater.*, 2024, DOI: **10.1007/s42765-024-00403-x**.

13 A. Raman, A. Sankar, A. S. D., A. Anilkumar and A. Saritha, Insights into the Sustainable Development of Lignin-Based Textiles for Functional Applications, *Macromol. Mater. Eng.*, 2022, **307**, 2200114, DOI: **10.1002/mame.202200114**.

14 J. Sunthornvarabhas, S. Liengprayoon, T. Lerksamran, C. Buratcharin, T. Suwonsichon and W. Vanichsriratana, *et al.*, Utilization of Lignin Extracts from Sugarcane Bagasse as Bio-based Antimicrobial Fabrics, *Sugar Technol.*, 2019, **21**(2), 355–363, DOI: **10.1007/s12355-018-0683-2**.

15 J. Petkovska, N. Mladenovic, D. Marković, M. Radoičić, N. A. Vest and B. Palen, *et al.*, Flame-Retardant, Antimicrobial, and UV-Protective Lignin-Based Multilayer Nanocoating, *ACS Appl. Polym. Mater.*, 2022, **4**(6), 4528–4537, DOI: **10.1021/acsapm.2c00520**.

16 O. Gordobil, R. Herrera, R. Llano-Ponte and J. Labidi, Esterified organosolv lignin as hydrophobic agent for use on wood products, *Prog. Org. Coat.*, 2017, **103**, 143–151, DOI: **10.1016/j.porgcoat.2016.10.030**.

17 S. S. Singh, A. Zaitoon, S. Sharma, A. Manickavasagan and L. T. Lim, Enhanced hydrophobic paper-sheet derived from Miscanthus × giganteus cellulose fibers coated with esterified lignin and cellulose acetate blend, *Int. J. Biol. Macromol.*, 2022, **223**(Pt A), 1243–1256.

18 E. L. Hult, J. Ropponen, K. Poppius-Levlin, T. Ohra-Aho and T. Tamminen, Enhancing the barrier properties of paper board by a novel lignin coating, *Ind. Crops Prod.*, 2013, **50**, 694–700, DOI: **10.1016/j.indcrop.2013.08.013**.

19 J. Ruwoldt, F. H. Blindheim and G. Chinga-Carrasco, Functional surfaces, films, and coatings with lignin – a critical review, *RSC Adv.*, 2023, **13**(18), 12529–12553. Available from: **https://pubs.rsc.org/en/content/articlehtml/2023/ra/d2ra08179b**.

20 J. Szulc, W. Machnowski, S. Kowalska, A. Jachowicz, T. Ruman and A. Steglińska, *et al.*, Beeswax-modified textiles: Method of preparation and assessment of antimicrobial properties, *Polymers*, 2020, **12**(2), 344, DOI: **10.3390/polym12020344**.

21 A. Lozhechnikova, H. Bellanger, B. Michen, I. Burgert and M. Österberg, Surfactant-free carnauba wax dispersion and its use for layer-by-layer assembled protective surface coatings on wood, *Appl. Surf. Sci.*, 2017, **396**, 1273–1281.

22 J. Janesch, B. Arminger, W. Gindl-Altmutter and C. Hansmann, Superhydrophobic coatings on wood made of plant oil and natural wax, *Prog. Org. Coat.*, 2020, **148**, 105891, DOI: **10.1016/j.porgcoat.2020.105891**.

23 S. Jeong, S. Beluns, O. Platnieks, J. Sevcenko, M. Jure and G. Gaidukova, *et al.*, Academic Editors: Cristiana Boi and membranes Sustainable Wax Coatings Made from Pine Needle Extraction Waste for Nanopaper Hydrophobization, *Membranes*, 2022, **12**(5), 537, DOI: **10.3390/membranes12050537**.

24 K. A. Henn, N. Forsman, T. Zou and M. Österberg, Colloidal Lignin Particles and Epoxies for Bio-Based, Durable, and Multiresistant Nanostructured Coatings, *ACS Appl. Mater. Interfaces*, 2021, **13**(29), 34793–34806.

25 N. Forsman, L. S. Johansson, H. Koivula, M. Tuure, P. Kääriäinen and M. Österberg, Open coating with natural wax particles enables scalable, non-toxic hydrophobation of cellulose-based textiles, *Carbohydr. Polym.*, 2020, **227**, 115363.

26 S. Javaid, A. Mahmood, H. Nasir, M. Iqbal, N. Ahmed and N. M. Ahmad, Layer-By-Layer Self-Assembled Dip Coating for Antifouling Functionalized Finishing of Cotton Textile, *Polymers*, 2022, **14**(13), 2540, DOI: **10.3390/polym14132540**.

27 A. Moreno, I. Pylypchuk, Y. Okahisa and M. H. Sipponen, Urushi as a Green Component for Thermally Curable Colloidal Lignin Particles and Hydrophobic Coatings, *ACS Macro Lett.*, 2023, **12**(6), 759–766, DOI: **10.1021/acsmacrolett.3c00186**.

28 K. A. Y. Koivu, H. Sadeghifar, P. A. Nousiainen, D. S. Argyropoulos and J. Sipilä, Effect of Fatty Acid Esterification on the Thermal Properties of Softwood Kraft Lignin, *ACS Sustainable Chem. Eng.*, 2016, **4**(10), 5238–5247.

29 T. Zou, M. H. Sipponen and M. Österberg, Natural shape-retaining microcapsules with shells made of chitosan-coated colloidal lignin particles, *Front. Chem.*, 2019, **7**, 1–12.

30 M. Farooq, T. Zou, J. J. Valle-Delgado, M. H. Sipponen, M. Morits and M. Österberg, Well-Defined Lignin Model Films from Colloidal Lignin Particles, *Langmuir*, 2020, **36**(51), 15592–15602.

31 N. Forsman, A. Lozhechnikova, A. Khakalo, L. S. Johansson, J. Vartiainen and M. Österberg, Layer-by-layer assembled hydrophobic coatings for cellulose nanofibril films and textiles, made of polylysine and natural wax particles, *Carbohydr. Polym.*, 2017, **173**, 392–402. Available from: **https://linkinghub.elsevier.com/retrieve/pii/S0144861717306446**.

32 M. Österberg, J. Vartiainen, J. Lucenius, U. Hippi, J. Seppälä and R. Serimaa, *et al.*, A fast method to produce strong NFC films as a platform for barrier and functional materials, *ACS Appl. Mater. Interfaces*, 2013, **5**(11), 4640–4647.

33 E. Kimiaei, M. Farooq, R. Grande, K. Meinander, M. Österberg and E. Kimiaei, *et al.*, Lignin Nanoparticles as an Interfacial Modulator in Tough and Multi-Resistant Cellulose-Polycaprolactone Nanocomposites Based on a Pickering Emulsions Strategy, *Adv. Mater.*, 2022, **9**, 2200988. Available from: **https://www.advmatinterfaces.de**.

34 T. Jyske, J. Liimatainen, J. Tienaho, H. Brännström, D. Aoki and K. Kuroda, *et al.*, Inspired by nature: Fiber networks functionalized with tannic acid and condensed tannin-rich extracts of Norway spruce bark show antimicrobial efficacy, *Front. Bioeng. Biotechnol.*, 2023, **11**, 1–20.

35 J. Tienaho, D. Reshamwala, T. Sarjala, P. Kilpeläinen, J. Liimatainen and J. Dou, *et al.*, Salix spp. Bark Hot Water Extracts Show Antiviral, Antibacterial, and Antioxidant Activities—The Bioactive Properties of 16 Clones, *Front. Bioeng. Biotechnol.*, 2021, **9**, 1228.

36 M. Dobrosielska, R. Dobrucka, P. Kozera, D. Brząkalski, E. Gabriel and J. Głowacka, *et al.*, Beeswax as a natural alternative to synthetic waxes for fabrication of PLA/diatomaceous earth composites, *Sci. Rep.*, 2023, **13**(1), 1–18. Available from: https://www.nature.com/articles/s41598-023-28435-0.

37 H. Setälä, H. L. Alakomi, A. Paananen, G. R. Szilvay, M. Kellock and M. Lievonen, *et al.*, Lignin nanoparticles modified with tall oil fatty acid for cellulose functionalization, *Cellulose*, 2020, **27**(1), 273–284.

38 M. P. C. Volpi, R. G. Bastos, A. P. R. Badan, M. H. A. Santana and V. S. Santos, Characterization of lignocellulosic composition and residual lipids in empty fruit bunches from palm oil processing, *Grasas Aceites*, 2019, **70**(3), 314, DOI: 10.3989/gya.0818182.

39 K. A. Henn, S. Babaeipour, S. Forssell, P. Nousiainen, K. Meinander and P. Oinas, *et al.*, Transparent lignin nanoparticles for superhydrophilic antifogging coatings and photonic films, *Chem. Eng. J.*, 2023, **475**, 145965.

40 H. Zhou, Q. Li, Z. Zhang, X. Wang and H. Niu, Recent Advances in Superhydrophobic and Antibacterial Cellulose-Based Fibers and Fabrics: Bio-inspiration, Strategies, and Applications, *Adv. Fiber Mater.*, 2023, **5**(5), 1555–1591, DOI: 10.1007/s42765-023-00297-1.

41 L. Dong, T. Nypelö, M. Österberg, J. Laine and M. Alava, Modifying the wettability of surfaces by nanoparticles: Experiments and modeling using the wenzel law, *Langmuir*, 2010, **26**(18), 14563–14566.

42 I. S. Bayer, D. Fragouli, P. J. Martorana, L. Martiradonna, R. Cingolani and A. Athanassiou, Solvent resistant superhydrophobic films from self-emulsifying carnauba wax-alcohol emulsions, *Soft Matter.*, 2011, **7**, 36. Available from: https://www.rsc.org/softmatter.

43 N. Forsman, A. Lozhechnikova, A. Khakalo, L. S. Johansson, J. Vartiainen and M. Österberg, Layer-by-layer assembled hydrophobic coatings for cellulose nanofibril films and textiles, made of polylysine and natural wax particles, *Carbohydr. Polym.*, 2017, **173**, 392–402.

44 Q. Wang, G. Sun, Q. Tong, W. Yang and W. Hao, Fluorine-free superhydrophobic coatings from polydimethylsiloxane for sustainable chemical engineering: Preparation methods and applications, *Chem. Eng. J.*, 2021, **426**, 130829.

45 V. Dichiarante, M. I. Martinez Espinoza, L. Gazzera, M. Vuckovac, M. Latikka and G. Cavallo, *et al.*, A Short-Chain Multibranched Perfluoroalkyl Thiol for More Sustainable Hydrophobic Coatings, *ACS Sustainable Chem. Eng.*, 2018, **6**(8), 9734–9743, DOI: 10.1021/acssuschemeng.8b00777. Available from:.

46 Y. Luo, S. Wang, X. Fu, X. Du, H. Wang and M. Zhou, *et al.*, Fabrication of a Bio-Based Superhydrophobic and Flame-Retardant Cotton Fabric for Oil–Water Separation, *Macromol. Mater. Eng.*, 2021, **306**(3), 2000624.

47 E. L. Hult, J. Ropponen, K. Poppius-Levlin, T. Ohra-Aho and T. Tamminen, Enhancing the barrier properties of paper board by a novel lignin coating, *Ind. Crops Prod.*, 2013, **50**, 694–700.

48 A. Mahdy, M. G. Mohamed, K. I. Aly, B. Ahmed and H. Emam, HE. Liquid crystalline polybenzoxazines for manufacturing of technical textiles: Water repellency and ultraviolet shielding, *Polym. Test.*, 2023, 119.

49 S. Afroz, M. A. R. Azady, Y. Akter, A. Al Ragib, Z. Hasan and M. S. Rahaman *et al.*, *Self-cleaning textiles: Structure, fabrication and applications*, Fundamentals of Natural Fibres and Textiles. Ltd, 2021, pp. 557–597.

50 S. Park, J. Kim and C. H. Park, Analysis of the wetting state of super-repellent fabrics with liquids of varying surface tension, *RSC Adv.*, 2016, **6**(51), 45884–45893. Available from: https://pubs.rsc.org/en/content/articlehtml/2016/ra/c5ra27281e.

51 A. Bashari, M. Shakeri and A. R. Shirvan, *UV-protective textiles, The Impact and Prospects of Green Chemistry for Textile Technology*, 2019, pp. 327–365.

52 A. Raman, A. Sankar, S. D. Abhirami, A. Anilkumar and A. Saritha, Insights into the Sustainable Development of Lignin-Based Textiles for Functional Applications, *Macromolecular Materials and Engineering*, John Wiley and Sons Inc, 2022, vol. 307.

53 L. Vevere, A. Fridrihsone, M. Kirpluks and U. Cabulis, A Review of Wood Biomass-Based Fatty Acids and Rosin Acids Use in Polymeric Materials, *Polymers*, 2020, **12**(11), 2706.

54 Y. Zhang and M. Naebe, Lignin: A Review on Structure, Properties, and Applications as a Light-Colored UV Absorber, *ACS Sustainable Chem. Eng.*, 2021, **9**(4), 1427–1442.

55 R. Gulati, S. Sharma and R. K. Sharma, Antimicrobial textile: recent developments and functional perspective, *Polymer Bulletin*, Springer Science and Business Media Deutschland GmbH, 2022, vol. 79, pp. 5747–5771.

56 T. Abdullah, T. Colombani, T. Alade, S. A. Bencherif and A. M. Memić, Injectable Lignin-*co*-Gelatin Cryogels with Antioxidant and Antibacterial Properties for Biomedical Applications, *Biomacromolecules*, 2021, **22**, 4110–4121.

57 A. G. Morena and T. Tzanov, Antibacterial lignin-based nanoparticles and their use in composite materials, *Nanoscale Adv.*, 2022, **4**(21), 4447–4469.

58 J. L. Espinoza-Acosta, P. I. Torres-Chávez, B. Ramírez-Wong, C. M. López-Saiz and B. Montaño-Leyva, Antioxidant, antimicrobial, and antimutagenic properties of technical lignins and their applications, *BioResources*, 2016, **11**(2), 5452–5481.

59 H. T. Yang, J. W. Chen, J. Rathod, Y. Z. Jiang, P. J. Tsai and Y. P. Hung, *et al.*, Lauric acid is an inhibitor of Clostridium difficile growth in vitro and reduces inflammation in a mouse infection model, *Front. Microbiol.*, 2018, **8**, 2635.

60 G. Casillas-Vargas, C. Ocasio-Malavé, S. Medina, C. Morales-Guzmán, R. G. Del Valle and N. M. Carballeira, *et al.*, Antibacterial fatty acids: An update of possible mechanisms of action and implications in the development of the next-generation of antibacterial agents, *Prog. Lipid Res.*, 2021, **82**, 101093.

61 C. J. Zheng, J. S. Yoo, T. G. Lee, H. Y. Cho, Y. H. Kim and W. G. Kim, Fatty acid synthesis is a target for antibacterial activity of unsaturated fatty acids, *FEBS Lett.*, 2005, **579**(23), 5157–5162.

62 J. H. Oh, T. J. Ko, M. W. Moon and C. H. Park, Nanostructured fabric with robust superhydrophobicity induced by a thermal hydrophobic ageing process, *RSC Adv.*, 2017, **7**(41), 25597–25604.
63 B. J. Ju, J. H. Oh, C. Yun and C. H. Park, Development of a superhydrophobic electrospun poly(vinylidene fluoride) web *via* plasma etching and water immersion for energy harvesting applications, *RSC Adv.*, 2018, **8**(50), 28825–28835.
64 F. J. Maksoud, M. Lameh, S. Fayyad, N. Ismail, A. R. Tehrani-Bagha and N. Ghaddar, *et al.*, Electrospun waterproof breathable membrane with a high level of aerosol filtration, *J. Appl. Polym. Sci.*, 2018, **135**(2), 2–9.
65 J. Wu, J. Li, Z. Wang, M. Yu, H. Jiang and L. Li, *et al.*, Designing breathable superhydrophobic cotton fabrics, *RSC Adv.*, 2015, **5**(35), 27752–27758.
66 F. J. Maksoud, M. Lameh, S. Fayyad, N. Ismail, A. R. Tehrani-Bagha and N. Ghaddar, *et al.*, Electrospun waterproof breathable membrane with a high level of aerosol filtration, *J Appl Polym Sci*, 2018, **135**(2), 45660, DOI: **10.1002/app.45660**.
67 Y. J. Ren and J. E. Ruckman, Water Vapour Transfer in Wet Waterproof Breathable Fabrics, *J. Ind. Text.*, 2003, **32**(3), 165–175.
68 G. R. Lomax, The Design of Waterproof, Water Vapour-Permeable Fabrics, *J. Ind. Text.*, 1985, **15**(1), 40–66.
69 S. Joshi, V. Midha and S. Rajendran, Multifunctional waterproof breathable coating on polyester-based woven protective clothing for healthcare application, *Prog. Org. Coat.*, 2023, **178**, 107482.